NIPES

Journal of Science and Technology Research

Journal homepage: www.nipesjournals.org.ng

Magnetic Moment Interpretation for the Large Hadron Collider (LHC) Generated Spin-0 and Spin- ½ Magnetic Monopoles

D. Dosu & O. Ebomwonyi
Department of Physics, University of Benin, Nigeria
Corresponding Author: osarodion.ebomwonyi@uniben.edu

Article Info

***Keywords*:**
Magnetic moment, Monopoles, Pseudorapidity,Efficiency analysis, Drell-Yan mechanism.

Received 18 April 2023
Revised 24 April 2023
Accepted 24 April 2023
Available online 06 June 2023

https://doi.org/10.5281/zenodo.8010047

Abstract

Through a comparative study of generated kinematics parameters such as transverse momentum, pseudorapidity and azimuthal distribution, this study proposes the magnetic moment as a novel parameter in the registration and detection of magnetic monopoles

1.0. Introduction

Paul Dirac's paper [1] on magnetic monopoles proposed the existence of particles that carry a single magnetic pole, either north or south. A revolutionary idea at the time because it implied that the fundamental building blocks of the universe were not just electric charges, as had been previously believed, but also magnetic charges. The paper questioned the validity of Maxwell's equations of classical electrodynamics for lack of symmetry in electromagnetic duality. Equation (1) to Equation (4) is the Maxwell's equations of classical electrodynamics.

$$\nabla . E = \frac{\rho_e}{\epsilon_0} \quad (1)$$

$$\nabla . B = 0 \quad (2)$$

$$\nabla \times E = -\frac{\partial B}{\partial t} \quad (3)$$

$$\nabla \times B = \mu_0 \epsilon_0 \frac{\partial E}{\partial t} \quad (4)$$

Dirac's compelling theoretical evidence fixes the asymmetry in Equation (1) and Equation (2) by positing that

$$\nabla . B = \rho_m \quad (5)$$

The symmetry between electric and magnetic fields in the source-free Maxwell's equations suggests the possibility of electric charges having magnetic counterparts known as magnetic monopoles. The symmetrized Maxwell's equations are invariant under rotation in the plane of the electric and magnetic fields, and direct observation of single magnetic monopoles will have far-reaching consequences, most notably an explanation of the electric-charge quantization.

According to Dirac [1], when a monopole moves through space, it generates a magnetic field around it. However, this field is singular at the location of the monopole, which is physically impossible. To resolve this problem, Dirac proposed the existence of a line-like defect called a Dirac string, which carries the singularity of the magnetic field. The monopole is located at the end of the string, and the field is non-singular everywhere else. Dirac's theory was based on the mathematical framework of quantum mechanics and relied on the existence of a particular type of field called a gauge field. The idea of magnetic monopoles was later incorporated into grand unified theories (GUTS); which attempt to unify the fundamental forces of nature.
The Dirac strings are hypothetical topological defects associated with magnetic monopoles in gauge theories and were introduced by Paul Dirac as a way to reconcile the existence of magnetic monopoles with the observed absence of singularities in the electromagnetic field.

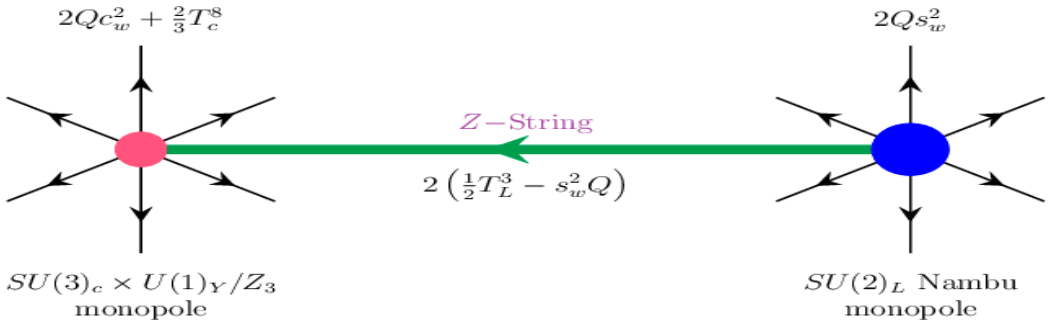

Fig. 1: A doubly charged colored Dirac monopole (pink) and a Nambu monopole (blue) connected by a Z-string with magnetic flux T [2]

Dirac further theorized that the quantization of electric charge could be understood as a consequence of angular momentum, with his argument deriving the quantization condition. The relationship between electric and magnetic charge is given as

$$ge = n\hbar c/2 \tag{6}$$

where g is the magnetic charge, e is the elementary charge, n is an integer, and $\hbar$ is the reduced Planck's constant. This could be extended to derive the fundamental magnetic charge on the mopnopole, called Dirac charge, to be

$$g_D = \hbar c/2e = e/2\alpha \tag{7}$$

Dirac's argument predicts the fundamental magnetic charge to be

$$q = Ng_D ec, \tag{8}$$

here, we have set q in SI units and g_D a dimensionless quantity, that is,

$$g_D = \frac{1}{2\alpha} = 68.5e \tag{9}$$

where $\alpha = \frac{1}{137}$ is the fine structure constant.

The force between a monopole and an anti-monopole is $(137/2)^2$, which is 4700 times greater than the force between an electron and a positron. This force between the monopole pairs is much stronger, hinting at the difficulty of finding these fermions in nature [3].

Grand Unified Theories extend beyond the standard model and aim at unifying the three gauge interactions SU(3), SU(2) and U(1). t'Hooft [4] showed that specific spontaneously broken gauge theories have non-singular classical solutions that lead to magnetic monopoles in quantum theory, hence independently predicting the existence of monopoles as a twist or knot defect in the GUT Higgs field.

Although the monopoles appearing in grand unification theories typically have masses of the order of the unification scale, $10^{16} GeV,$ some extensions of the standard model predict electroweak monopoles (which obey Schwinger's quantization condition that $g_2 q_1 - g_1 q_2 = \frac{2nh}{\mu_0}$) with masses as low as $4TeV$. Possibilities of generating monopoles of different mass scales have been predicted via stages of symmetry breaking

$$SO(10) \xrightarrow{M_1} SU(4) \times SU(2) \times SU(2) \xrightarrow{M_2} SU(3) \times SU(2) \times SU(1).$$

If monopoles were to exist, we expect they would have a unique magnetic moment that would be distinct from that of other magnetic particles. By measuring the magnetic moment of a sample, it would be possible to identify the presence of monopoles and determine their properties, such as their spin, mass, and charge. These monopoles would be very massive and would have been produced in large numbers in the early universe, but would be very rare today due to their large mass. The mass of the magnetic monopole is a hypothetical particle treated as a free parameter. When considering the Dirac monopole, a parameter that is readily considered due to its known ionizing property is the dE/dx significance measurement. The rack registered due to dE/dx is a parabolic path, curved in the $r-z$ plane due to the candidate's interaction with the magnetic field in the inner tracker detector.

The transfer of momenta in an individual interaction then depends on the charge and mass of the target particle, the velocity and charge of the projectile, and the impact parameter generated during the collision. The general equation which gives information about energy deposition is known as the Berthe-Bloch equation

$$-dE/dx = K \frac{Z}{A} \frac{Z^2}{\beta^2} [l \frac{2m_e c^2 \beta^2 \gamma^2}{I} - \beta^2] \tag{10}$$

In the case of a monopole such as the one produced at the LHC; we consider them to be a relatively heavy particle with a mass of the border of a few TeV. Such a monopole is expected to lose energy only through ionization [5]. With charge $q_m = gec$ **,** the Berthe-Bloch equation is modified for the monopole to become

$$-dE/dx = K \frac{Z}{A} g^2 [l \frac{2m_e c^2 \beta^2 \gamma^2}{I_m} + \frac{K(|g|)}{2} - \frac{1}{2} - B(|g|)] \tag{11}$$

To make important deductions, we consider the kinematics parameters; pseudorapidity, transverse momentum and azimuthal distribution for spin models 0 and ½. Due to the dependence of the detector acceptance on both the energy and angular distributions of monopoles, the cross-sections are subject to certain constraints that are influenced by specific theoretical models. The spin-0 monopole, being scalar, has no magnetic moment while the spin- ½ fermionic monopole couples minimally with its magnetic moment generated through spin interaction. Furthermore, the spin- ½

magnetic monopole models are augmented by the presence of spinor magnetic moment terms with an introduced dimensionless phenomenological parameter $\tilde{k} = 0$ [6].
Dirac monopoles were predicted to be the source of a singular magnetic field [1]. These sources were analyzed in effective field theory to be matter fields with spins 0, ½, and 1 [7]. However, it is important to note that the paper does not provide any specific implications beyond this; hence his paper offers experimental evidence for the case of the magnetic moment as a deciding parameter in the registrations of spin-0 and spin- ½ monopole candidates in the ECAL. Plots for generator-level kinematics were compared for the compact muon solenoid (CMS)-generated monopole masses, which ranged from 1 TeV to 4.5 TeV. We also compared the results for efficiency analysis.

2.0 Methodology

The Compact Muon Solenoid (CMS) experiment is one of four detectors built at the crossing sites of the LHC beams and is one of two general-purpose detectors (the other being ATLAS) that have been designed to explore the physics opportunities presented by the LHC. Thus, the initial goal of the CMS detector is to study several Higgs boson production modes, which can be explored with the detector. The detector has a beam spacing of 25 ns, and beam crossing occurs in the CMS detector at a rate of 40 million per second (40 MHz). An additional complication is the approximately 25 interactions that occur with each beam crossing - this generates 1 billion events in the CMS detector every second. To extract physics from these interactions, it is vital to have fast electronics and very good resolution (proton-proton interactions are very messy and produce hundreds or thousands of particle candidates), and because these events occur far too quickly to all be recorded and would take up vast amounts of disk space to store what are, for the majority, uninteresting events, very precise "triggering" is required.

2.1 Monopole Signature and Identification in the CMS Detector

2.1.1. Data generation cycles, analysis and Monte-Carlo experiment

The ultimate aim of this experiment, data generation cycles, and analysis are to ensure that only the monopole's signature gets registered in the electromagnetic calorimeter (ECAL)

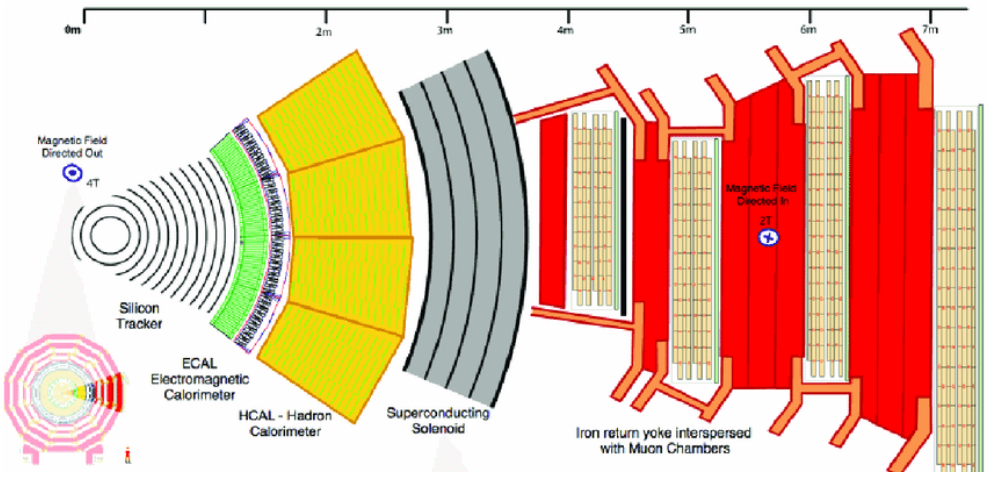

Fig. 2: CMS Detector [8]

2.2 Analysis Strategy

2.2.1 Monopole Tracking Recognition

This analysis strategy uses a track combiner algorithm, instead of the SM-oriented standard tracking algorithm because the monopole behaves differently from standard model (SM) particles.

2.2.2 Track Ionization

We then proceed to measure the ionization of the track as identified via the TCA. The monopole, due to its high mass, can be easily predicted by the Berthe relationship to deposit energy at a high rate, hence it's dE/dx measurement is high. The background noise is also factored in, and instead of the standard dE/dx which is an harmonic average of dE/dx, we instead measure dE/dx significance, which is a combination of the total number of strips and fractions of unsaturated strips [3].

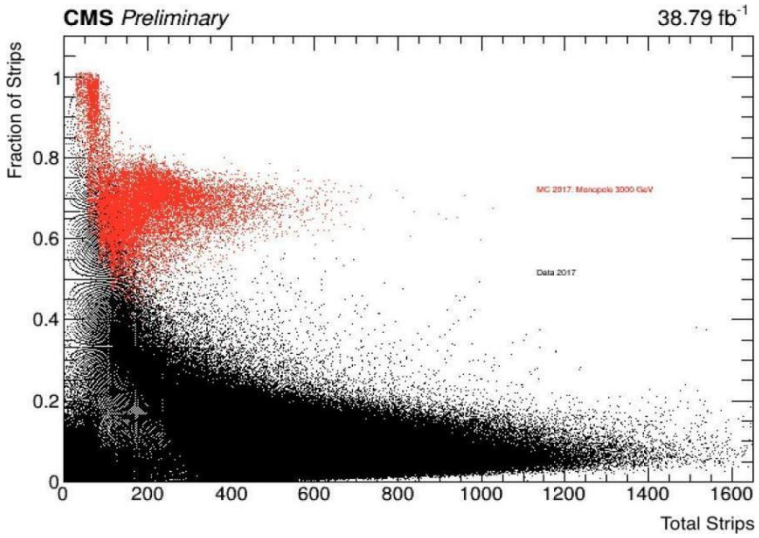

Fig. 3: Applying the dE/dx significance cut shows a clearer discrepancy from the standard dE/dx cut

2.2.3 Track Curvature

Relatively small curvature in the track path is observed for monopoles with energy high enough to transverse the electromagnetic calorimeter; this explains why the $r-z$ curvature recorded in the tracks of monopoles is quite insignificant.

2.2.4 Electromagnetic Calorimeter Cluster Finding

It is expected that the monopole candidates studied in this analysis will lose most if not all, of their energy in the ECAL due to the ionization we have described. Also, a consequence of having almost all its energy deposited in the ECAL is the next layer in the CMS detector set-up. The Hadronic Calorimeter (HCAL) will register few or no monopole deposits. The cluster shape for monopole candidates is tracked in the ECAL crystals using two clustering algorithms: the Hybrid algorithm and the Island algorithm. The monopole, unlike the SM particles that deposit their energy in several crystals, deposits all of its charge (about 5000 times that of the electron) in the ECAL, what this implies is that the ratio of seed crystal energy to that in the 5 x 5 crystal will approximate to 1. The Island and Hybrid algorithms are used for this analysis.

2.2.5 Trigger Selection

HLTPhoton200 v* was used for 2017 and 2018 datasets, with traverse energy (ET) as $200GeV$. It is worth mentioning too, that due to the L1 spike killer algorithm, the analysis considers monopole candidates that do not deposits all their energy into the central crystal.

2.2.6 Monopole Identification

In addition to the aforementioned parameters, we require that the distance between the monopole track and the extrapolated ECAL cluster be less than 0.5. We then bring these characteristics together to form the basis of our selection criteria:

Table 1: Pre-selection cuts for monopole matching

Pre-Selections	Parameter	Cut
Parabolic Fit	$\|RZPar0\| \rightarrow Z_0 = \|d\|$	< 10 cm
	$\|RZPar1\| \rightarrow \eta_0 = \|f\|$	< 999 cm
	$\|RZPar2\| \rightarrow \rho - Z$ curvature $= \|g\|$	0.005 cm^{-1}
Matching Fit	$\triangle R$	< 0.5
	HCAL Isolation	< 10 GeV
Circular Fit	$\|XYPar0\| \rightarrow d = \sqrt{(a-c)^2 + b^2} - \|c\|$	< 0.6 cm
	$\|XYPar2\| \rightarrow \|\Phi_0 - arctan\frac{b}{c-a}\|$	< 10

Table 2: Analysis selection cut applied to identify monopole candidates that passed the pre-test

	Parameter	Threshold
Analysis Cuts	Energy Deposit in the ECAL	> 200 GeV
	HLT_Photon200_v^*	Pass
Loose Cuts	dE/dx_{Sig}	≥ 7
	$F51$	> 0.60
Discriminating Cuts	dE/dx_{Sig}	≥ 9
	$F51$	> 0.85

The CMS experiment simulates, analyzes, and reconstructs data using specialized software referred to as CMS software (CMSSW). To create MC simulations and reconstruct data chosen by the trigger system, the CMSSW combines algorithms. This search takes into account processes like PDFs, harmonization, underlying events, and parton showers to produce the necessary output. [3]

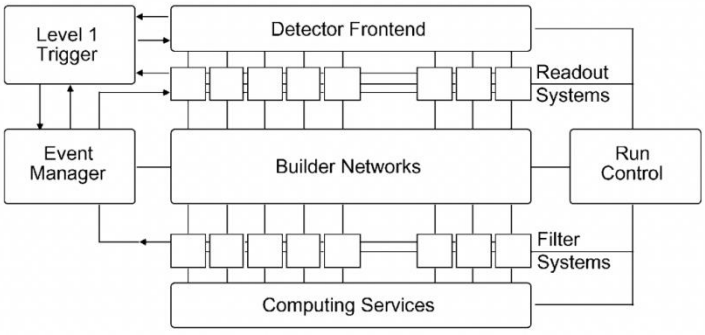

Fig. 4: CMS trigger and data acquisition system

2.2.7 Signal Efficiency

The signal efficiency analysis is done in the order that the loose pre-selection (trigger selection and then the energy cut) are first applied. Monte Carlo samples for the full RUN II for mass points 1

TeV to 4.5 TeV were generated to study the selection efficiency. The candidates that pass these cuts are then checked against the tighter selection of dE/dx signal and F51, where,

$$Relative\ efficiency = \frac{number\ of\ events\ after\ selections}{number\ of\ events\ after\ selections\ except\ the\ mentioned\ cut} \quad (12)$$

$$Signal\ efficiency = \frac{number\ of\ events\ after\ all\ selection\ cuts}{number\ of\ events\ after\ selections\ before\ selections\ applied} \quad (13)$$

3.0 Results and Discussion

Table 3: Efficiency analysis result for spin- ½ mass 1000*GeV*

1000 Photon200	CutFlow	Relative eff		1000 NoTrg	CutFlow	Relative eff
Generated ev	16889			Generated ev	16889	
TRG	773	4.58%		TRG	16844	99.73%
QualityCuts	759	98.19%		QualityCuts	13997	83.10%
ECut	684	90.12%		ECut	5741	41.02%
F51Cut	368	53.80%		F51Cut	4785	83.35%
dEdXSigCut	366	99.46%		dEdXSigCut	4738	99.02%
Signal efficiency	0.0216709		0.0011204152	Signal efficiency	0.280538	
	0.04576943573					
	N1Cuts				N1Cuts	
No TRG	5035	0.0726912		No TRG	5035	0.941013
No Quality	520	0.703846		No Quality	5674	0.835037
No ECut	598	0.61204		No ECut	8706	0.544222
No F51Cut	673	0.543834		No F51Cut	5631	0.841414
No dEdXSig	485	0.754639		No dEdXSig	5093	0.930296

Table 4: Efficiency analysis result for spin-0 mass 1000*Gev*

Spin 0	1000 HLT_Photon200	CutFlow	Relative efficiency			CutFlow	Relative efficiency
	Generated ev	9500			1000 NOTRG		
	TRG	859	0.09042105		Generated eV	9500	
	QualityCuts	847	0.98603		TRG	9492	99.91%
	ECut	803	0.94805		Quality cuts	8878	93.53%
	F51Cut	449	0.55915		ECuts	5910	66.57%
	dEdXSigCut	448	0.99777		F51Cuts	4875	82.49%
	Signal efficiency	0.0471579			dEdxsigCut	4833	99.14%
					Signal efficiency	0.508737	
		N1Cuts	Relative eff				
	No TRG	5216	0.0858896		N1Cuts		Relative efficiency
	No Quality	607	0.738056		No TRG	5216	0.926572
	No ECut	692	0.647399		No Quality	5503	0.878248
	No F51Cut	800	0.56			7416	0.651699
	No dEdXSig	586	0.764505			5837	0.827994
						5277	0.915861

Table 5: Efficiency analysis result for spin- ½ mass 2000*GeV*

2000 Photon200	CutFlow	Relative eff		2000 NoTrg	CutFlow	Relative eff
Generated ev	17629			Generated ev	17629	
TRG	1028	5.83%		TRG	17584	99.74%
QualityCuts	1009	98.15%		QualityCuts	15014	85.38%
ECut	930	92.17%		ECut	7319	48.75%
F51Cut	537	57.74%		F51Cut	5955	81.36%
dEdXSigCut	531	98.88%		dEdXSigCut	5873	98.62%
Signal efficiency	0.0301208		0.00128729545	Signal efficiency	0.333144	
	0.05723523739					
	N1Cuts				N1Cuts	
No TRG	6320	0.084019		No TRG	6320	0.929272
No Quality	709	0.748942		No Quality	6835	0.859254
No ECut	776	0.684278		No ECut	9430	0.6228
No F51Cut	911	0.582876		No F51Cut	7143	0.822204
No dEdXSig	684	0.776316		No dEdXSig	6419	0.91494

Table 6: Efficiency analysis result for spin-0 mass 2000*GeV*

2000 Photon200	CUTFLOW	RELATIVE EFFICIENCY		2000 NO TRG	CUT FLOW	RELATIVE EFFICIENCY
GENERATED eV	14000			GENERATED eV	14000	
TRG	1420	10.143		TRG	13992	99.943
QUALITY CUT	1411	99.366		QUALITY CUT	13278	94.897
ECUT	1333	94.47		ECUT	9912	74.649
F51CUT	764	57.314		F51CUT	8059	81.305
DeDxSIG_CUT	759	99.345		DEDXSIG_CUT	7970	98.896
SIGNAL EFFICIENCY	0.0542143			SIGNAL EFFICIENCY	0.569286	
	CUTFLOW	RELATIVE EFFICIENCY		2000 NO TRG	CUT FLOW	RELATIVE EFFICIENCY
NO TRG	8791	86.338		NO TRG	8791	90.661
NO QUALITY	1032	73.547		NO QUALITY	9191	86.715
NO ECUT	1097	69.189		NO ECUT	10972	72.6394
NO F51CUT	1318	57.587		NO F51CUT	9768	81.593
NO DEDXSIG	1011	75.074		NO DEDXSIG	8913	89.419

Table 7: Summary of efficiency analysis results for both spin- ½ and spin-0

1000GeV	Spin-1/2 (16889 entries)	Spin-0 (9500 entries)
TRG	4.58%	9.042%
F51	53.80%	55.92%
dE/dXsigcut	99.46%	99.78%
2000GeV	Spin-1/2 (17629 entries)	Spin-0 (14000 entries)
TRG	5.83%	10.14%
F51	57.74%	57.31%
dE/dXsigcut	98.88%	99.35%

3.1 Generator Level Kinematics

The generated kinematics plot for monopole data sets 1000*GeV*-4500*GeV* is displayed in the plots for transverse and total momentum distribution for spin- ½ monopole candidates.

3.2 Pseudorapidity

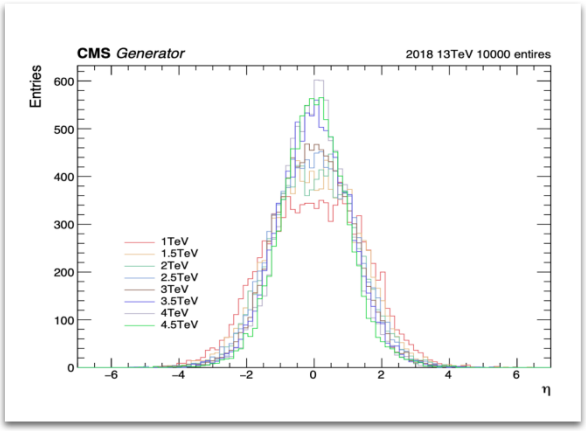

Fig. 5: Spin- ½ monopole

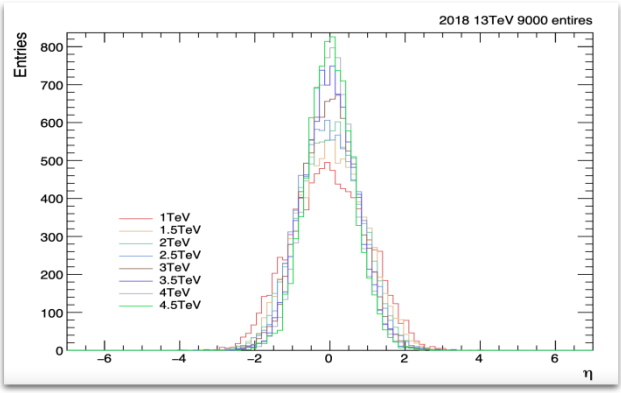

Fig. 6: Spin-0 monopole

3.3 Transverse momentum

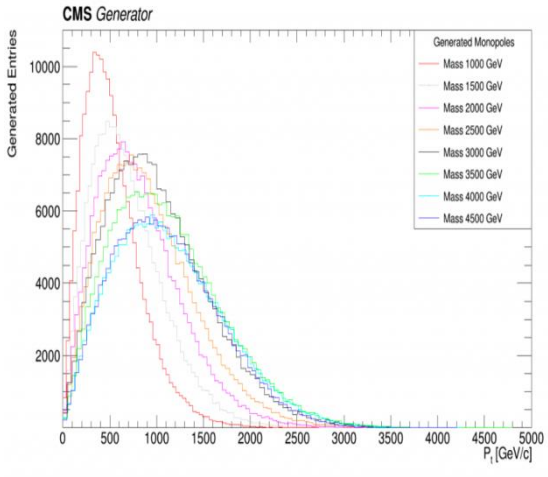

Fig. 7: Spin- ½ monopole

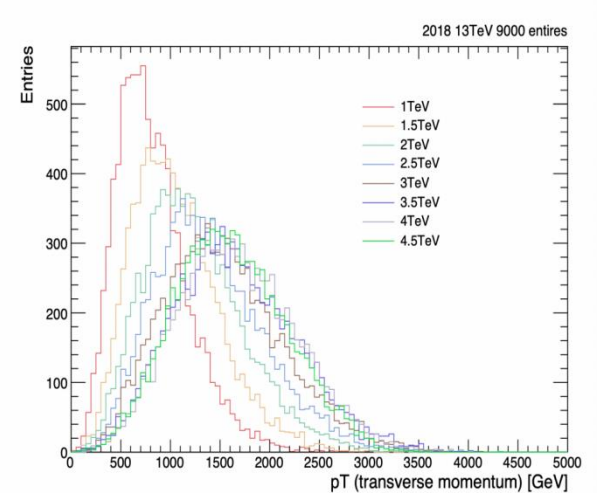

Fig. 8: Spin-0 monopole

3.4 Azimuthal distribution (ϕ)

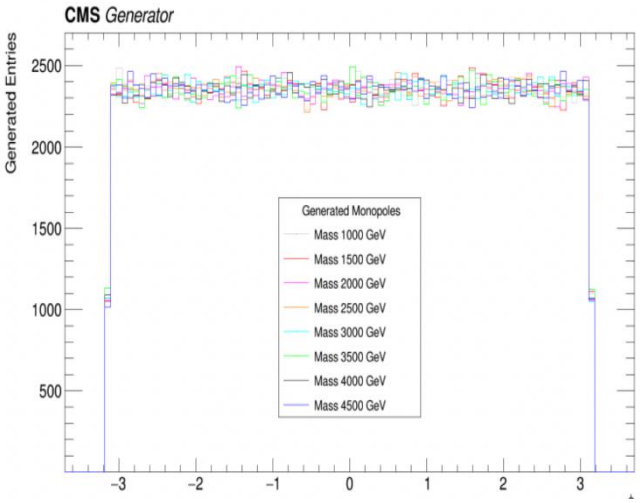

Fig. 9: Spin- ½ monopole

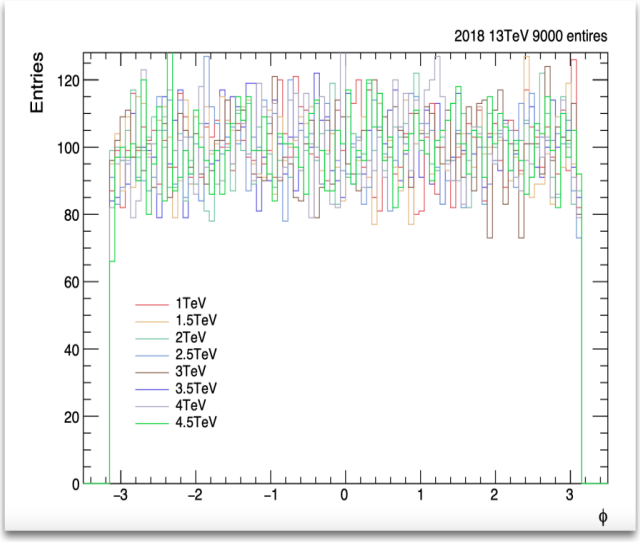

Fig. 10: Spin-0 monopole

From the results of the efficiency analysis shown in Tables 3 to 6, we observe that the offline selection cuts have efficiencies greater than 50% and 90% for F51 and dE/dx significance, respectively. Also, the trigger selection for spin- ½ has efficiency lower than 10%, even after the offline selections are applied (Table 7). We present two mass points; 1000 *GeV* and 2000 *GeV*, to explain a question that may arise from comparing the relatively lower number of generated entries for the 1000 *GeV* spin-0 mass. The closeness in range for the 2000 *GeV* mass shows that the efficiency of registration for the spin-0 monopole candidate is higher than the spin- ½ irrespective of the number of generated entries.

In Figures 5 and 6, the plotted histogram for pseudorapidity is seen to have a harder registration and is more centrally registered ($-2 < \eta < 2$) for the spin-0 monopole than in the case of the spin- ½ monopole ($-3 < \eta < 3$).

In Figures 7 and 8, it is seen that monopoles have high transverse momentum; also the registration for the spin-0 monopole is again observed to be harder than that of spin- ½. No difference except for harder registration in the case of spin-0 monopoles is observed in the azimuthal distributions (Figures 9 and 10) due to the expected conservation of azimuthal symmetry. We conclude that the

observed higher efficiencies of the spin-0 monopole candidates are a consequence of it being a scalar particle, thereby causing it to not interact with the tracker system as would the spin- ½ fermionic monopoles.

4.0. Conclusion

This paper focuses how a magnetic monopole could account for the quantization of electric charge and symmetries, the electromagnetic equations proposed by Maxwell, and how theories beyond the standard model readily predict the magnetic monopole. We highlight the significance of magnetic moments as a crucial factor in how spin-0 and spin-½ monopole candidates are registered in the electromagnetic calorimeter (ECAL). This is supported by ROOT-generated plots for pseudorapidity, azimuthal distribution, and transverse momentum. We also compare the cases in the efficiency analysis to further reinstate the conjecture.

Data availability

All the data and codes used to produce the results presented in this paper are stored on CERN's lxplus server or on their GitLab platform.

Acknowledgment

I wish to thank my supervisors as a summer student at CERN: Albert De Roeck, Mai El Sawy, Srimanob Noraphat, Afsar Abbas and Lin Shih, for introducing me to the research area and for guidance. I also acknowledge the CERN and the CMS department for the data used in this work.

References

[1] P.A.M. Dirac (1931). Quantised singularities in the electromagnetic field. Proc. Roy. Soc. A 133, 60-72.
[2] G. Lazarides, Q. Shafi (2019). Monopoles, strings, and necklaces in SO(10) and E_6. Journal of High Energy Physics 139 (1-20).
[3] M.M. Hassan El Sawy (2020). Search for Magnetic Monopoles in the CMS experiment at the Large Hadron Collider (LHC). https://cds.cern.ch/record/2744867.
[4] G. 't Hooft (1974). Magnetic Monopoles in Unifified Theories. Magnetic monopoles in unifified gauge theories. Nucl. Phys. B 79, 276–284.
[5] A. De Roeck, A. Katre, P. Mermod, D. Milstead, T. Sloan (2012). Sensitivity of LHC experiments to exotic highly ionising particles. The European Physical Journal C 72. 1434-6052.
[6] S. Baines, N.E. Mavromatos, V.A. Mitsou, J.L. Pinfold, A. Santra (2018). Monopole production via photon fusionand Drell-Yan processes: MADGRAPH implementation and perturbativity via velocity-dependent coupling and magnetic moment as novel features. Eur. Phys. J. C 78: 966, doi:10.1140/epjc/s10052-018-6440-6.
[7] S. Baines (2019). Effective Field Theory Treatment of Monopole Production by Drell–Yan and Photon Fusion for Various Spins.https://doi.org/10.3390/proceedings2019013001.
[8] A. Seiden (2012). Characteristics of the ATLAS and CMS detectors. Phil. Trans. R. Soc. A370, 892–906.